Comblike Poly(α-alkyl γ-glutamate)s: Computer Simulation Studies of an Intermediate Thermal Phase

David Curcó,† David Zanuy, Carlos Alemán,* Elisabet Rude,† and Sebastián Muñoz-Guerra

Departament d'Enginyeria Química, E.T.S. d'Enginyers Industrials de Barcelona, Universitat Politècnica de Catalunya, Diagonal 647, Barcelona E-08028, Spain

Received October 16, 2002

Monte Carlo (MC) simulations have been used to study the structure of an intermediate thermal phase of poly(α-octadecyl γ,D-glutamate). This is a comblike poly(γ-peptide) able to adopt a biphasic structure that has been described as a layered arrangement of backbone helical rods immersed in a paraffinic pool of polymethylene side chains. Simulations were performed at two different temperatures (348 and 363 K), both of them above the melting point of the paraffinic phase, using the configurational bias MC algorithm. Results indicate that layers are constituted by a side-by-side packing of 17/5 helices. The organization of the interlayer paraffinic region is described in atomistic terms by examining the torsional angles and the end-to-end distances for the octadecyl side chains. Comparison with previously reported comblike poly(β-peptide)s revealed significant differences in the organization of the alkyl side chains.

Introduction

Helical comblike polypeptides are of interest because of their peculiar structure.[1] These polymers are constituted by two different structural units: (i) a rigid helical backbone, which is stabilized by intramolecular hydrogen bonds, and (ii) a flexible long linear alkyl side chain, the conformation of which mainly depends on the temperature. As a result, comblike polypeptides adopt a biphasic structure, which consists of a layered arrangement of backbone helical rods immersed in a paraffinic pool (Figure 1). This structure is highly sensitive to temperature, so phase transitions are usually induced by heating or cooling treatments. The main structural differences between these phases concern the organization of the alkyl side chains in the paraffinic region. In the most ordered phase, denoted A, the alkyl side chains are partially crystallized in a hexagonal lattice with the interior methylene units in trans conformation. Phase A converts into phase B upon heating above the transition temperature, T_1. In phase B, the alkyl side chains are in a molten state even though the polypeptide main chains retain the helical conformation and the layered arrangement. A third phase C is observed at higher temperatures in certain cases, but the structure present in this phase is not well understood.

A notable effort was dedicated in the last 2 decades to investigate the structure of comblike poly(γ-alkyl α,L-glutamate)s, that is, the alkyl esters of poly(α-glutamic acid), abbreviated PGALG-*n* (where *n* indicates the number of carbon atoms of the alkyl side chain).[1−3] Recently, we evidenced that helical comblike poly(β-peptide)s behave similarly to PGALG-*n*.[4−8] More specifically, poly(α-alkyl β,L-aspartate)s, abbreviated PAALA-*n*, were examined by

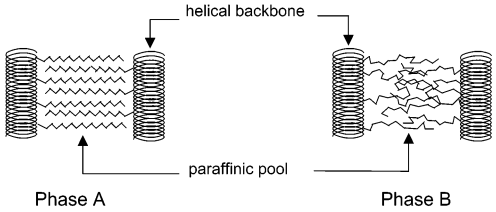

Figure 1. Schematic model illustrating the phases A and B of comblike polypeptides.

differential scanning calorimetry, NMR, and X-ray diffraction and shown to adopt the characteristic biphasic structure with the polypeptide chains in 13/4 helical conformation.[4−6] Furthermore, an atomistic structural description was provided for comblike PAALA-*n* by using Monte Carlo (MC) simulations.[5−8]

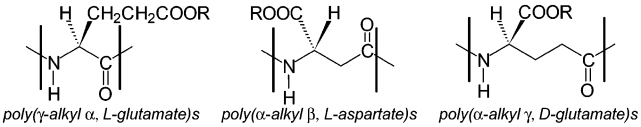

On the other hand, the synthesis and structure of poly(α-alkyl γ-glutamate)s with short and long alkyl side chains, abbreviated PAAG-*n*, have been examined by us.[9−12] These poly(γ-peptide)s were prepared either by chemical synthesis or by derivatization of bacterially produced poly(γ-glutamic acid) with different D/L enantiomeric ratios. A recent analysis of the microstructure of these biosynthetic polymers by ^{13}C NMR revealed that they are actually stereocopolymers made of enantiomerically homogeneous D and L blocks.[10] Accordingly, optically pure polymers and racemic polymers exhibited practically the same structural behavior.

Two series of PAAG-*n* differing in the D/L enantiomeric ratio, 9:1 and 1:1, and with *n* ranging from 12 to 22 were synthesized and characterized by a variety of experimental techniques.[9a] In a preceding paper, a detailed experimental

* To whom correspondence should be addressed. E-mail: carlos.aleman@upc.es.

† On leave from Departament d'Enginyeria Química, Facultat de Química, Universitat de Barcelona, Martí i Franques 1, Barcelona E-08028, Spain.

10.1021/bm025702q CCC: $25.00
Published on Web 00/00/0000

study is carried out on the supramolecular structure adopted by these comblike poly(γ-glutamate)s with particular attention paid to the phase transitions that take place by effect of temperature.[9b] The observations were consistent with the occurrence of a biphasic layered structure, the layers being constituted by helices stabilized by intramolecular hydrogen bonds. Such results along with those previously obtained for poly(β-peptide)s establish that this type of supramolecular assemblies is not found only for α-helix but that it is shared by other nonconventional polypeptides provided that they can be arranged in a helical conformation. The investigation of PAAG-*n* is particularly interesting because of the biosynthetic accessibility and potential biodegradability of their parent compound, poly(γ-glutamic acid) (PGGA). Accordingly, the structure of PAAG-*n* deserves a microscopic study using atomistic simulations.

The purpose of this work is to provide a detailed description of the atomistic structure of comblike PAAG-*n* using advanced MC methods. The study has been confined to the study of the structure of phase B because of (i) the difficulty of MC technique to reproduce the crystallized region of phase A, (ii) the almost total lack of experimental information on the structure of phase C, and (iii) the amount of experimental data available on phase B that, although insufficient to attain a detailed description of the structure adopted in this phase, is very useful for supporting the simulation analysis. Simulations have been performed considering the enantiomerically pure poly(α-octadecyl γ,D-glutamate), denoted PAADG-18, for consistency with our previous studies on PAALA-18.[5,7,8] Furthermore, a detailed comparison between helical comblike poly(β-peptide)s and poly(γ-peptide)s has been made.

Model and Computational Methods

Helical Conformation. Precise experimental information required to define the helical backbone conformation of comblike polypeptides is not usually attained because of the constitutional complexity of these systems. For comblike poly(α-peptide)s and poly(β-peptide)s, the molecular conformation was inferred from the X-ray data obtained for members with short alkyl side groups, which crystallize in a three-dimensional array.[1,2,4] Accordingly, 18/5 and 13/4 helical conformations were proposed for comblike PGALG-*n* and PAALA-*n*, respectively. In the present study, we have initially considered the helical conformations previously described for poly(γ-glutamic acid) and poly(γ-glutamate)s bearing short side chains. Experimental observations first carried out by Rydon,[15] and later by other authors, evidenced that poly(γ,D-glutamic acid) adopts a helical conformation.[16,17] Computer simulations revealed recently that such experimental data are compatible with a left-handed 17/5 helix stabilized by intramolecular hydrogen bonds set between the amide groups i and $i + 3$.[18] On the other hand, synthetic methyl and benzyl esters of poly(γ,L-glutamic acid) were found to adopt a 5/2 helical conformation stabilized by intramolecular hydrogen bonds between the i and $i + 2$ amide groups.[11,12] Solution NMR experiments carried out on related oligo(γ,L-amino acid)s detected the same conformation.[13,14] More recently, a third helical conformation has been described for the benzyl ester of biosynthetic poly(α-benzyl γ,L-glutamate).[12] This consists of a 37/10 helix with the same hydrogen-bonding scheme and rise per residue (1.50 Å) as the 17/5 helix, which make both helices very close in topology. In fact, the maximum difference between dihedral angles of the 17/5 and 37/10 helices is only 4.1°. Given the strong similarities between these two helices and the high computing cost that the analysis of the 37/10 helix would imply, only the 5/2 and 17/5 helical arrangements were considered in this study. However, it should be emphasized that results obtained with the 17/5 helix are perfectly applicable to the 37/10 helix because of their structural similarity. The main characteristics of the 5/2, 17/5, and 37/10 helices are summarized in Table 1. Figure 2 shows the axial and equatorial projections of 5/2 and 17/5 helices examined in the present work.

Table 1. Conformational Angles and Hydrogen-Bonding Parameters for the Helical Conformations Considered in This Work

	helix		
	5/2	17/5	37/10
dihedral angles[a]			
φ	−137.9	70.9	70.9
ξ_1	53.0	52.8	53.6
ξ_2	75.6	−171.0	−172.8
ψ	−143.8	159.9	164.0
ω	180.0	180.0	180.0
η	180.0	155.0	157.0
rise per residue[b]	2.02	1.50	1.50
helix sense	right-handed	left-handed	left-handed
H-bond type	intramolecular	intramolecular	intramolecular
H-bond scheme[c]	C═O(i)···H−N($i + 2$)	N−H(i)···O═C($i + 3$)	N−H(i)···O═C($i + 3$)
d(H···O)[b]	1.82	1.90	2.02
∠N−H···O[a]	164.8	167.0	165.1
atoms per H-bond	14	19	19

[a] In deg. [b] In Å. [c] The label indicated in parentheses corresponds to the number of amide group.

Molecular Models. The structure of comblike PAADG-18 in the solid state was simulated by packing four independent helices of PAADG-18 in an orthogonal simulation box with the helices oriented with their axes parallel to the *z*-axis (Figure 3). The *x*-axis was defined as pointing along the line joining centers of neighboring helices within a layer. The *y*-axis pointed therefore perpendicular to the helix layers, and these were parallel to the $x-z$ plane. Independent chains in the arrangements constituted by 5/2 and 17/5 helices contained a total of 10 (5×2) and 17 residues in each one, respectively. Periodic boundary conditions were applied along the three axes by using the minimum image convention.

All of the methylene and end methyl groups were represented using pseudoatoms, while the remaining atoms were described explicitly. The number of explicit atoms/pseudoatoms comprising a typical simulation of PAADG-18 varied with the helical backbone conformation, being 1160 and 1972 for the 5/2 and 17/5 helices, respectively. Bond lengths and angles were kept fixed for the alkyl side chains, whereas bond lengths and angles and torsional angles were kept fixed for all helices, which is consistent with the

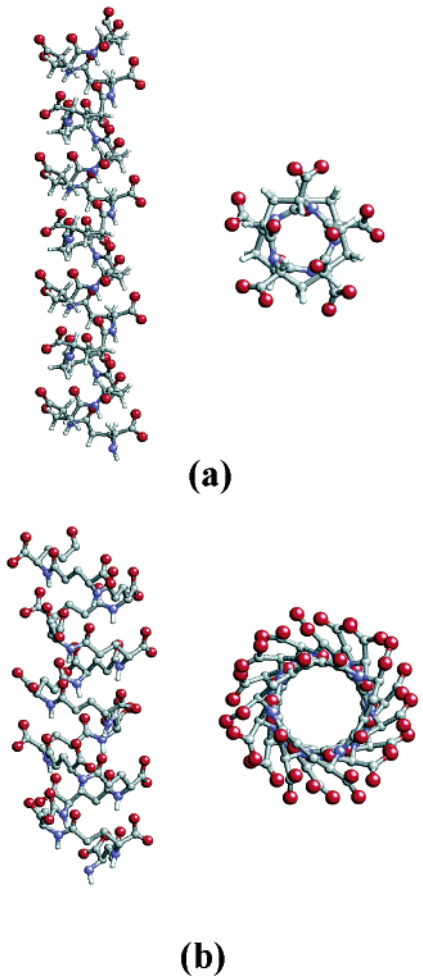

Figure 2. Axial and equatorial projections of (a) the 5/2 and (b) the 17/5 helices considered for PAADG-18. To clarify the figure, the octadecyl side groups have not been represented.

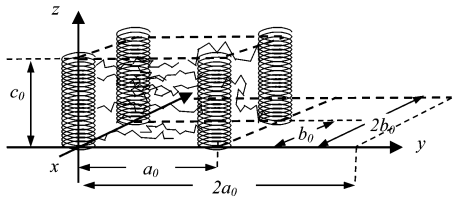

Figure 3. Schematic representation of the simulated models. The cell parameters b_0 and a_0 correspond to the separation between helices within a layer and between two successive layers, respectively. The dimensions of the simulation box for the different models investigated were $2a_0$, $2b_0$, and c_0.

experimental observation that helical conformations are retained in phases A and B.[9]

Simulation Details. Simulations were performed using an advanced MC sampling technique, configurational bias Monte Carlo (CBMC).[19,20] The CBMC method consists of the following three steps: (i) a chain is selected at random; (ii) the chain is cut at a random position; (iii) the chain is sequentially regrown bond-by-bond by examining a number of possible torsions (N_s), which are randomly chosen. This algorithm was specifically adapted for studying comblike polymers and subsequently implemented into a computed program denoted MCDP (Monte Carlo Simulations of Dense Polymers).[21] In addition to CBMC moves, a small fraction of Metropolis moves was also considered for the alkyl side chains. In the CB algorithm, $N_s = 8$ torsional angles were used to sample the torsional space for the side chains. The degrees of freedom in simulations of *NVT*-type, tht is, without varying the size of the simulation box, were the torsional angles of the alkyl side chains and the setting angles, which define the relative orientation among the helices. On the other hand, in *NPT*-type simulations ($P = 1$ atm), the dimensions of the simulation box were also considered as degrees of freedom. The frequency used for the different types of MC moves, the number of steps, and temperature of the system for all of the simulations presented below are displayed in Table 2.

Table 2. Temperature, Number of Steps, and Frequency (%) for the Different Types of Monte Carlo Moves in *NVT* and *NPT* Simulations

simul	model	T^a	type	steps	CB[b]	Metrop[b]	a/b[c]	θ[d]
1	5/2-A	348	*NVT*	7.5×10^4	0.6	0.1		0.3
2	5/2-P	348	*NVT*	7.5×10^4	0.6	0.1		0.3
3	5/2-A	348	*NPT*	2.5×10^5	0.55	0.05	0.2	0.2
4	5/2-P	348	*NPT*	2.5×10^5	0.55	0.05	0.2	0.2
5	17/5-A	348	*NVT*	7.5×10^4	0.6	0.1		0.3
6	17/5-P	348	*NVT*	7.5×10^4	0.6	0.1		0.3
7	17/5-A	348	*NPT*	2.5×10^5	0.55	0.05	0.2	0.2
8	17/5-P	348	*NPT*	9×10^5	0.55	0.05	0.2	0.2
9	17/5-P	348	*NVT*	3.5×10^5	0.6	0.1		0.3
10	17/5-P	363	*NVT*	5×10^5	0.55	0.05		0.4

[a] Temperature in K. [b] Frequency of CB and Metropolis moves for the alkyl side chains. [c] Frequency of *NPT* moves. [d] Frequency of moves for the setting angles of the helices.

The Amber force field was used to represent the electrostatic, van der Waals, and torsional energies of the system.[22] The van der Waals energy was computed in the usual pairwise additive mode using a Lennard-Jones 6-12 potential. The van der Waals parameters, σ and ϵ, were computed using arithmetic and geometric mean combining rules, respectively.

Electrostatic interactions play a major role in PAADG-*n* helix conformation; they are actually responsible for their high stability. Because we are comparing the stability of the 5/2 and 17/5 helices in supramolecular biphasic structures, these interactions were taken into account by assigning partial atomic charges to the atoms of both the backbone and side ester groups. Such electrostatic charges were derived by fitting the rigorously defined quantum mechanical molecular electrostatic potential, which was calculated at the ab initio HF/6-31G(d) level on a reduced model constituted by two residues, to the Coulombic electrostatic potential. This procedure was used for two reasons. First, previous studies demonstrated that in general the parameters derived from suitable reduced models lead to reliable results.[23] Second, the electrostatic parameters derived at the HF/6-31G(d) level have been included in the libraries of the Amber force fields.[22] However, electrostatic interactions were neglected for the mobile alkyl side chains because they can be considered as electrically neutral. This strategy, which is efficient from a computational point of view, was proved to be reliable for comblike PAALA-*n*.[8] Thus, calculations including the electrostatic interactions for the alkyl side groups led essentially to the same results as those in which such interactions were omitted. Furthermore, it should be noted that electrostatic interactions are usually neglected in

both molecular dynamics and MC simulations of melts of alkyl chains.[24]

Electrostatic interactions for the partially charged atoms were evaluated using a standard Coulombic potential. It is expected that such a simple approach produces reliable results for the following reasons. First, the atomic charges on the backbone atoms are relatively low because no anion/cation is included in the system. Furthermore, the distance between neighboring polymer helices is considerably large. Nonbonding interactions were truncated at 15 Å, implying that all atoms of one residue interact with all other atoms of another residue if at least one pair of atoms is within this limit. A three-term Fourier series expansion was used to represent the torsional energy. Nonbonding and torsional parameters were taken from Amber 4.0 libraries.[25]

It should be mentioned that during the last years several force fields have been optimized for the simulation of long paraffinic chains.[26] Within this context, the anisotropic united atom force field developed by Toxvaerd[26a,b] and co-workers deserves special attention. This model, which allows the movement of the interaction center on each segment depending on the conformation of the whole molecule, was successful in predicting the equation of state and dynamics of alkanes, as well as the structure and thermodynamics of Langmuir monolayers. However, it should be noted that MC simulations of PAADG-18 should provide a satisfactory description not only of the paraffinic interphase but also of the polypeptide chains. The Amber force field is able to satisfy such requirements,[5−8] and for this reason, we decided to use it. Furthermore, previous studies indicated that the behavior of long alkyl chains can be also correctly simulated using simple isotropic force fields.[19,24]

The atomistic modeling of the phase A was performed by using the graphical tools implemented in the Cerius 2 computer package.[27]

Results and Discussion

The Helical Conformation in Comblike PAADG-18. For each helix type, two different packing modes were considered: (i) the chains arranged antiparallel with respect to each other (A) and (ii) the chains arranged in parallel (P). The initial dimensions of the simulation box for the two packing modes of 5/2 helices, henceforth denoted 5/2-A and 5/2-P models, were $2a_0 = 56.00$, $2b_0 = 24.21$, and $c_0 = 20.20$ Å (Figure 3). Unfavorable interactions were removed by 7.5×10^4 MC steps of *NVT*-type at $T = 348$ K (simulations 1 and 2 in Table 2), this temperature being about 20 K higher than that observed for the phase A−B thermal transition in PAADG-18.[9] After this, production runs consisting of 2.5×10^5 steps of *NPT*-type at the same temperature were started (simulations 3 and 4 in Table 2), the atomic coordinates being saved at 2500 steps intervals. To consider the influence of the starting point in the simulations, additional calculations were performed for the 5/2-A and 5/2-P models by varying both the dimensions of the simulation box and the arrangement of the helices (data not shown). However, such simulations do not deserve any extra discussion because they provided similar results to those presented below.

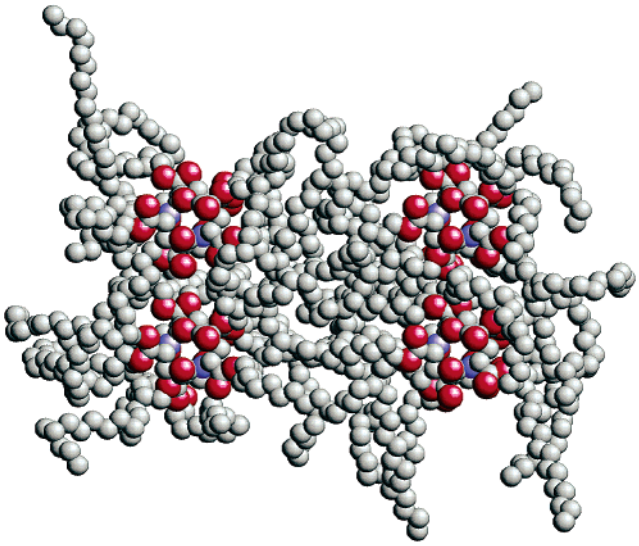

Figure 4. Equatorial projection ($x-y$ plane) of a representative microstructure provided by MC simulations of *NPT*-type for the 5/2-P model of PAADG-18.

Both the 5/2-A and 5/2-P models were found to evolve toward a structure in which the alkyl side chains are completely molten. Inspection of the recorded microstructures indicated that the side chains of adjacent residues were very separated, so they cannot pack favorably. As a consequence, the paraffinic side chains wrap around the helical backbones and large voids appeared in the middle part of the interlayer region. These features are illustrated in Figure 4, which shows a representative microstructure projected along the *c*-axis for the 5/2-P model.

The deficiencies detected for models 5/2-A and 5/2-P must be attributed to the structural characteristics of the 5/2 helix (Table 1). Consecutive side chains are spaced too far apart because of both the large rise per residue (2.02 Å) and the small number of residues per turn (2.5 residues turn^{-1}), which induce their folding toward the polypeptide backbone. The absence of interdigitation among the alkyl side chain of different helices is in contradiction with experimental evidences for PAADG-*n*,[9] and also PGALG-*n* and PAALA-*n*.[1−6]

Figure 5a shows the evolution of the energy through the *NPT* simulations for the two packing modes constituted by 5/2 helices. As can be seen, no significant energy difference appears between the 5/2-A and 5/2-P models, even though the 5/2-P model is slightly more stable (∼1 kcal/mol) than the 5/2-A. On the other hand, the evolution of the interlayer distance, a_0, through the simulations is displayed in Figure 5b. As can be seen, the interlayer distance a_0 decreases from 28 to 25.5 and 24.5 Å for the 5/2-A and 5/2-P, respectively. These values are about 5 Å shorter than the parameter experimentally measured for the phase B of PAADG-18 ($a_0 = 30$ Å).[9] Regarding the distance between neighboring helices within the same layer, b_0, it fluctuates around the initial value to arrive to ∼11.8 Å at the end of the simulation (data not shown). We are aware that the parameter a_0 is not completely equilibrated after 2.5×10^5 MC steps for the 5/2-P model. Nevertheless, in our opinion neither the 5/2-A nor the 5/2-P models deserve further consideration. Thus,

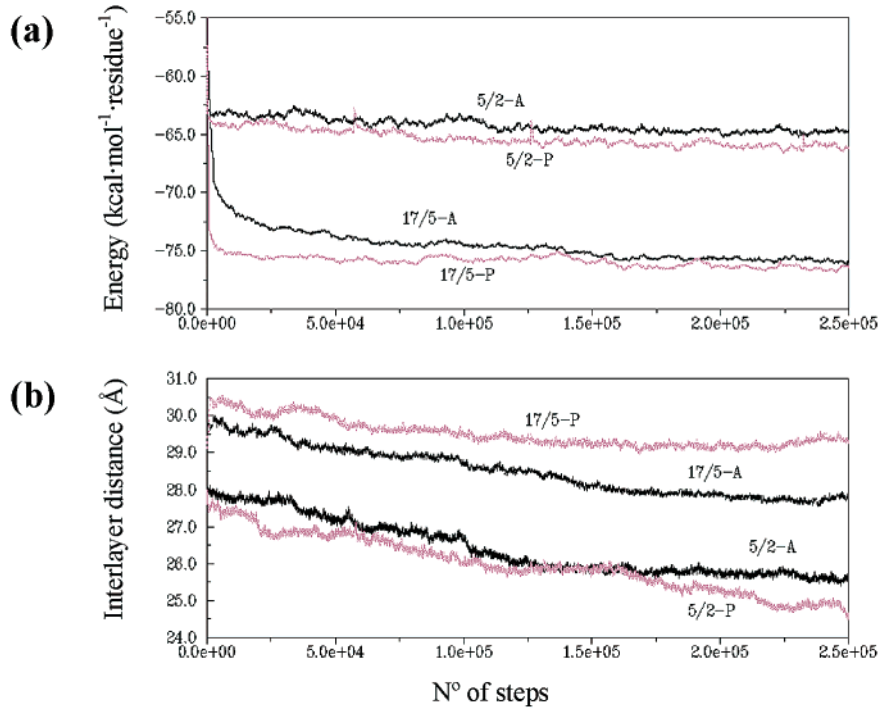

Figure 5. Evolution of (a) the energy and (b) the interlayer distance, a_0, through the *NPT* MC simulations (T = 348 K) for the 5/2-A, 5/2-P, 17/5-A, and 17/5-P models.

the overall results allow us to conclude that the models constituted by 5/2 helices provide a poor description of both the cell dimensions and the distribution of the alkyl side chains in the paraffinic interphase.

To investigate the second helical conformation considered in this study, the two packing modes of helices 17/5, denoted 17/5-A and 17/5-P models, were immersed in a simulation box with dimensions $2a_0$ = 58.00, $2b_0$ = 28.60, and c_0 = 25.50 Å. In this case, the parameters $2a_0$ and $2b_0$ were increased with respect to those initially considered for the 5/2-A and 5/2-P model. Otherwise unfavorable steric clashes were obtained because the diameter of the 17/5 helix is 1.8 Å larger than that of the 5/2 helix. In a first stage, MC simulations of *NVT*-type at T = 348 K were performed to minimize unfavorable sterical clashes (simulations 5 and 6 in Table 2). Next, simulations of *NPT*-type were performed at the same temperature (simulations 7 and 8 in Table 2).

It is worth noting that the interlayer distance a_0 sharply increases during the first hundredths of MC steps (Figure 5b). This enlargement is due to some unfavorable interactions that remained after *NVT* simulations. Subsequently, a_0 shortens slowly until reaching an equilibrium value. This is about 28 and 30 Å for the 17/5-A and 17/5-P models, respectively, revealing a good agreement with the experimental measure (a_0 = 30 Å). On the other hand, the parameter b_0 stabilizes at about 14 Å (data not shown), this value being similar to that used as starting point. It should be noted that no experimental value has been reported for b_0. The density calculated for this structure is about 1.0 g mL^{-1}, which is in comfortably good agreement with the value that should be experimentally expected. Note that the density measured for phase A is 1.02 g mL^{-1}. According to the contraction happening in the structure when phase A converts into phase B, the density of the latter would be increased by

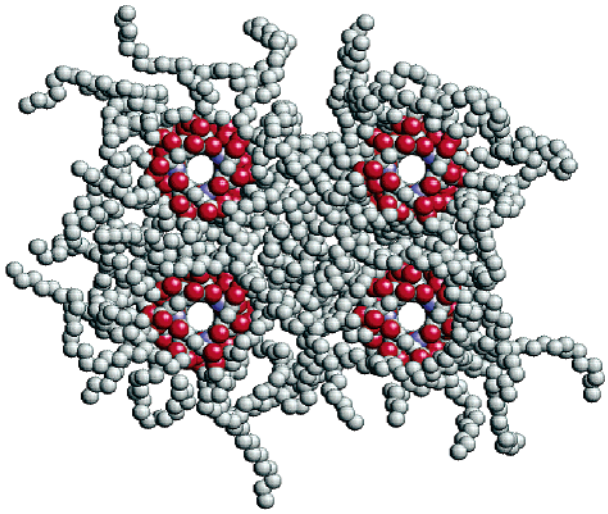

Figure 6. Equatorial projection ($x-y$ plane) of a representative microstructure provided by MC simulations of *NPT*-type for the 17/5-P model of PAADG-18.

6%. Indeed, the small difference (less than 10%) between the theoretical and experimental densities should be attributed to the Amber force field, which was optimized to study biological macromolecules in dilute solution.[22] Similar trends were detected in our previous studies on comblike PAALA-*n*.[6−8]

Figure 6 shows a representative microstructure of the 17/5-P model obtained in the production stage. As can be seen, the appearance of void spaces at the center of the paraffinic region is minimized because side chains are interdigitated, which is in good agreement with experimental data.[9] Comparison with the results obtained for the 5/2-A and 5/2-P models indicates that the shape and size of the core defined by the helix backbone plays a crucial role. Thus, the 17/5

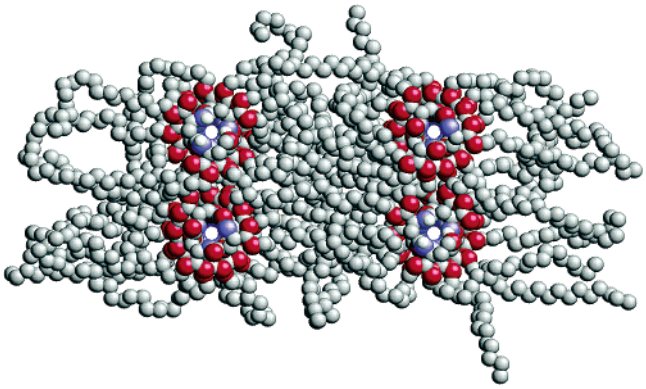

Figure 7. Equatorial projection ($x-y$ plane) of a representative microstructure provided by MC simulations of *NPT*-type for the phase B of PAALA-18.

helix presents a rise per residue of 1.50 Å, and its projection can be described as cylindrical. These characteristics allow both favorable interactions among the interdigitated side chains, because they are close in the space, and a homogeneous distribution of the side chains in the bending region, that is, the region in the proximity of the helix backbone.

The evolution of the energy after equilibration of the structures made of 17/5 helices is shown in Figure 5a. Again, no significant energy difference appears between the parallel and antiparallel models, the 17/5-P model being only slightly more favored than the 17/5-A one. However, an important energy gap (larger than 12 kcal mol^{-1} residue^{-1}) is observed when the models constituted by 17/5 and 5/2 helices are compared. The overall results lead us to consider that the 17/5 helix is more suitable for the formation of the biphasic structures of PAAGD-18 than the 5/2 one. Furthermore, we considered the 17/5-P packing for subsequent analyses even though no clear difference can be established between the parallel and the antiparallel models. For this purpose, simulation 8 was extended to 9 $\times$ 10^5 MC steps, no significant change being found in the lattice dimensions and the energy with respect to the results displayed in Figure 5.

A detailed inspection of the microstructures generated for the 17/5 models allows detection of a notable disorder in the interlayer region (Figure 6). Accordingly, the phase B of PAADG-18 can be conceived as layers of polypeptide helices embedded in a matrix made up of paraffinic chains in a molten state. This is a striking difference with respect to the phase B of comblike PAALA-*n*, in which the alkyl side chains retain a preferential alignment along the *y*-axis, that is, the side chains are partially disordered but not in the actual molten state.[6,7]

Furthermore, another important difference concerning the side-by-side arrangement of the helices appears between comblike poly(β-peptide)s and poly(γ-peptide)s. In the former case, neighboring helices within a layer were almost in contact. Thus, the alkyl side chains were essentially located in the interlayer region. Figure 7 shows a microstructure of PAALA-18, which was also obtained using MC simulations.[8] Conversely, the layers of PAADG-18 are constituted by polypeptide helices separated by alkyl side chains in a molten state, that is, the paraffinic chains are distributed between both the inter- and intralayer regions. However, the intralayer paraffinic region is so thin that neighboring helices are able to interact through their dipoles. Indeed, the cell dimensions derived from MC simulations clearly reflect the existence of such interaction. Thus, the parameters reached after 9 $\times$ 10^5 MC steps follow the pattern displayed in Figure 5b: a_0 ($\sim$30 Å) $\approx 2b_0$ ($\sim$2 $\times$ 14 Å). It should be emphasized that in the absence of such interactions the system should spontaneously evolve toward a new isotropic structure with parameters $a_0 \approx b_0$. The latter arrangement is that supposed to exist in the phase C of PAALA-18, which is reached upon heating the phase B upon a second transition temperature T_2.[4]

The differences between the phase B of PAADG-18 and PAALA-18 should be attributed to the topological differences that derive from the constitutional and conformational characteristics of these compounds. Comblike poly(β-peptide)s adopt a 13/4 helix with 3.25 residues per turn, while a 17/5 helix with 3.4 residues per turn is here assumed for PAADG-18. Furthermore, consecutive amide groups are separated along the main chain by two and three carbon atoms in PAALA-*n* and PAADG-*n*, respectively. Accordingly, the backbone and side ester atoms of each helix are closer in the former compounds than in the latter ones. This feature explains the presence of alkyl side chains between adjacent helices within the layers and the higher disorder found in the interlayer region.

Comparison with Phase A. The structural conclusions drawn for the phase B concerning the suitability of the 17/5 helical arrangement should be expected to be even more conspicuous for phase A because in this case the topological restrictions are more severe. Previous studies in comblike PAALA-*n* indicated that unconstrained MC simulations are not suitable to reproduce the phase A.[7] The failure to reproduce the crystallization of the paraffinic chains is due to the MC method itself. It is well-known that MC simulations of alkanes below the experimental melting point lead to supercooled liquids rather than to crystals.[28]

To provide an atomistic model of phase A comparable with phase B modeled by MC methods, we employed the graphical modeling tools implemented in the Cerius2 computer program.[27] Thus, one of the microstructures derived in the previous section for the 17/5-P model was used as starting point, both the cell dimensions and the torsional angles of the alkyl side chains being adjusted to fulfill the features derived from the experimental data. This process was combined with single-point energy calculations to avoid unfavorable interactions in the resulting model.

Figure 8 shows the atomistic model proposed for phase A of PAADG-18, which is characterized by the presence of order in the tree-axis. Even though this highly ordered structure fits the most important experimental trends reported for the phase A (density and crystallization of about eight methylene groups in the interlayer region), it should be only considered a rough atomistic model. This is because the conformational space of the dihedral angles involved in the side chain bending regions has not been explored. Unfortunately, the limitations of the MC techniques and the lack of experimental data concerning the side group arrangement in such regions does not allow us to obtain a more precise model.

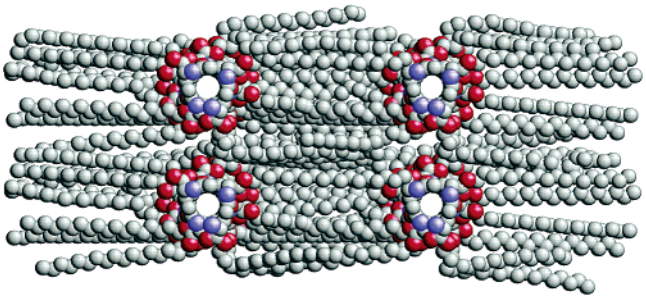

Figure 8. Representative structure of the phase A of PAADG-18 with main chains in the 17/5 helical conformation.

Organization of the Paraffinic Chains in Phase B of PAADG-18. To provide a more quantitative description of the structure of the paraffinic region in the phase B of PAADG-18, the 18 torsional angles for the alkyl side chains of the 17 × 4 residues explicitly considered were examined. For this purpose, additional simulations of *NVT*-type consisting of 3.5×10^5 steps were performed at $T = 348$ and 363 K for the 17/5-P model (simulations 9 and 10 in Table 2). According to the results presented in previous sections, the parameters of the simulation box were $2a_0 = 60.0$, $2b_0 = 28.0$, and $c_0 = 25.5$ Å.

The short-distance properties (at a level of 1−10 Å) of the alkyl side chains were examined by considering the first and second degree autocorrelation functions ($f_{1;bcf}$ and $f_{2;bcf}$, respectively), which allow us to study how fast the local properties of the paraffinic phase change as the MC simulations run. These were computed using the following expressions:[29]

$$f_{1;bcf}(n) = \langle v_i(j) v_i(j+n) \rangle_{i,j}$$

$$f_{2;bcf}(n) = \frac{3}{2} \langle (v_i(j) v_i(j+n))^2 \rangle_{i,j} - \frac{1}{2}$$

where the subscripts i and j correspond to the bonds and to the microstructures, respectively, and v_i is the unit vector of the ith bond. These functions estimate how fast the bonds erase the memory of the previous local configuration. The decay of both $f_{1;bcf}(n)$ and $f_{2;bcf}(n)$ at $T = 348$ K is shown in Figure 9, the autocorrelation functions obtained at $T = 363$ K (data not shown) being similar. The bond autocorrelation functions $f_{1;bcf}(n)$ and $f_{2;bcf}(n)$ drop to about 0.7 and 0.6, respectively. It should be remarked that for the system investigated, one of the ends of the side chain is anchored to the helix backbone precluding a complete loss of both short- and large-range correlations. According to this and to the results displayed in Figure 9, the microstructures obtained in the present simulations should be considered as statistically independent.

Figure 10 shows a population analysis for each torsional angle, the conformations being grouped in the following four categories: trans, gauche$^+$, gauche$^-$, and the other remaining conformers. The trans is the predominant conformation at the two temperatures, which is consistent with the results obtained for comblike PAALA-*n*.[6−8] On the other hand, the frequency of trans conformation slightly decreases with the temperature, that is, about 5% in average. This is not a surprising result because the population of folded states is expected to increase with the temperature.

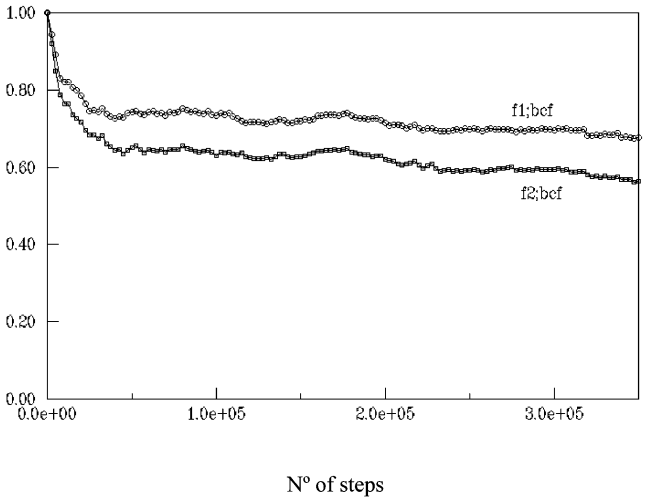

Figure 9. Bond autocorrelation functions ($f_{1;bcf}$ and $f_{2;bcf}$) for the phase B of PAAG-18 at $T = 348$ K.

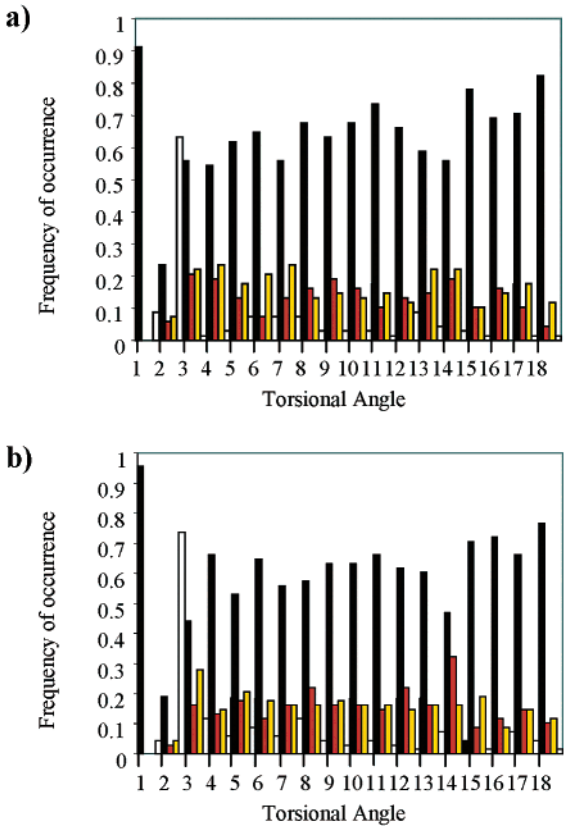

Figure 10. Torsional angle distribution for the alkyl side chains of PAADG-18 at (a) $T = 348$ K and (b) $T = 363$ K (b). The population analysis of the torsional angle associated with each of the 18 bonds in the alkyl side chain is specified. The four categories considered for each bond, in the order displayed in the figure from left to right, are trans, gauche$^+$, gauche$^-$, and the remaining conformers.

There is a fundamental difference between the results reported for PAALA-18 and those derived in the present work for PAADG-18. In comblike PAALA-18, the six torsional angles closer to the main chain helix present notable conformational differences with respect to the remaining 12 torsional angles. This feature was related with the alignment of the alkyl side chains along the *y*-axis. Conversely, for the compound under study, no significant difference is perceived in the populations of the last 16 torsional angles, for which

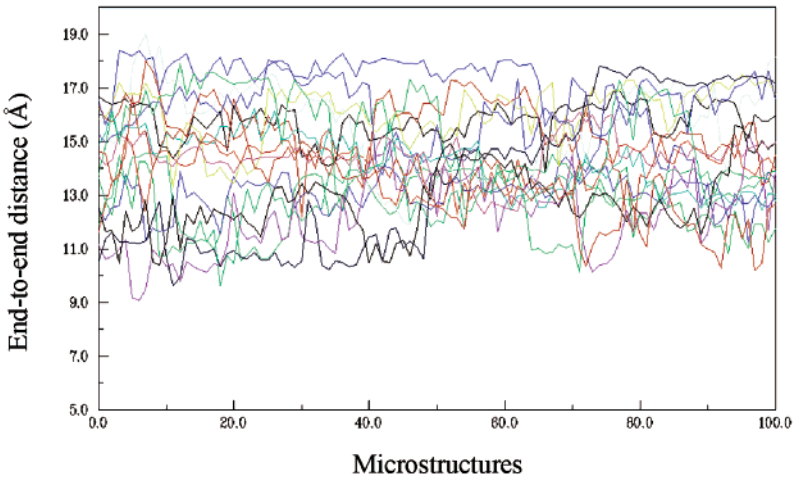

Figure 11. Evolution of the end-to-end distance for the alkyl side chains of PAADG-18 at $T = 348$ K. Every line corresponds to one of the 17 residues explicitly considered.

a homogeneous conformational distribution was found. This is consistent with the disordered state detected in the paraffinic interphase for the phase B in comblike poly(γ-peptide)s (see Figure 6).

To provide a more detailed view of the homogeneous distribution of the conformational preferences, the distance between the carbon atom of the ester group and the end methyl pseudoatom of the alkyl side chain, that is, the end-to-end distance of the paraffinic chains, was measured for each residue. Figure 11 shows the evolution of such distance for the 17 residues of the helix by considering the last 100 microstructures generated in the simulations at $T = 348$ K.

The computed values change with the position of residue within the layer varying from 11 to 18.5 Å. However, in general, the predominant values are those ranging from 13 to 16 Å, which indicates that, on average, the different side chains present similar conformational preferences. Moreover, comparison between the end-to-end distances at 348 and 363 K (data not shown) reveals that, in general, this parameter tends to decrease when the temperature increases. This behavior is in agreement with the population analyses displayed in Figure 10.

Summary

The structure of comblike PAADG-18 has been investigated using atomistic Monte Carlo simulations. A standard nonoptimized force field has been used together with a fixed bond length, fixed bond angle model. The CB algorithm, which was specially adapted to simulate comblike polymers, has been used through the MCDP computer program.[21]

Results indicate that the most favored model corresponds to a parallel packing of 17/5 helices. This helical conformation is the model previously put forward for poly(γ,L-glutamic acid), which is very similar to the 13/4 and α-helix proposed for PAALA-*n* and PGALG-*n*, respectively. The model would be perfectly replaceable by the 37/10 helix, the helix that has been found to exist in poly(α-benzyl γ,DL-glutamate). On the other hand, the organization of the paraffinic phase was examined by analyzing both the dihedral angles of the alkyl side chains and the end-to-end distance. The structure of comblike PAADG-*n* can be envisaged therefore as layers of rigid 17/5 helices separated by a molten paraffinic interphase. The differences detected between the paraffinic interphase of comblike PAADG-*n* and that found for PAALA-*n* can be considered one of the outstanding results of this paper.

Acknowledgment. The authors are greatly indebted to the Centre Europeu de Paralelisme de Barcelona (CEPBA) for computational facilities. This work was supported by DGICYT with Grant No. 3QU20000990.

References and Notes

(1) Loos, K.; Muñoz-Guerra, S. In *Supramolecular Polymers*; Cifferri, A., Ed.; Marcel Dekker, Inc.; New York, 2000; pp 263−321.
(2) Watanabe, J.; Ono, H.; Uematsu, I.; Abe, A. *Macromolecules* **1985**, *18*, 2141.
(3) Daly, W. H.; Negulescu, I. I.; Russo, P. S.; Poche, D. S. In *Macromolecular Assembies in Polymer Systems*; Shoever, P., Balazs, A. C., Eds.; ACS Symposium Series 493; American Chemical Society: Washington, DC, 1992; pp 292−299.
(4) López-Carrasquero, F.; Montserrat, S.; Martínez de Ilarduya, A.; Muñoz-Guerra, S. *Macromolecules* **1995**, *28*, 5535.
(5) Muñoz-Guerra, S.; López-Carrasquero, F.; Alemán, C.; Morillo, M.; Castelleto, V.; Hamley, I. *Adv. Mater.* **2002**, *14*, 203.
(6) Zanuy, D.; Alemán, C.; López-Carrasquero, F.; Báez, M. E.; García-Álvarez, M.; Laso, M.; Muñoz-Guerra, S. *Macromol. Chem. Phys.* **2001**, *202*, 564.
(7) Zanuy, D.; Namba, A. M.; León, S.; Alemán, C.; Muñoz-Guerra, S. *Polymer* **2001**, *42*, 281.
(8) León, S.; Alemán, C.; Muñoz-Guerra, S.; Laso, M. *J. Theor. Comput. Polym. Sci.* **2000**, *10*, 177.
(9) Morillo, M.; Martínez de Ilarduya, A; Muñoz-Guerra, S. *Macromolecules* **2001**, *34*, 7868; *Macromolecules*, submitted for publication, 2002.
(10) Martínez de Ilarduya, A.; Ittobane, N.; Bermúdez, M.; Alla, A.; El Idrissi, M.; Muñoz-Guerra, S. *Biomacromolecules*, in press.
(11) Puiggalí, J.; Muñoz-Guerra, S.; Rodríguez-Galán, A.; Alegre, C.; Subirana, J. A. *Makromol. Chem., Macromol. Symp.* **1988**, *20/21*, 167.
(12) Melis, J.; Zanuy, D.; Alemán, C.; García-Álvarez, M.; Muñoz-Guerra, S. *Macromolecules*, in press.
(13) Hintermann, T.; Gademann, K.; Jaun, B.; Seebach, D. *Helv. Chim. Acta* **1998**, *81*, 983.
(14) Bremmer, M.; Seebach, D. *Helv. Chim. Acta* **2001**, *84*, 1181.
(15) Rydon, H. N. *J. Chem. Soc.* **1964**, 1328.
(16) He, L. M.; Neu, M. P.; Vanderberg, L. A. *Environ. Sci. Technol.* **2000**, *34*, 1694.
(17) Sanda, F.; Fujiyama, T.; Endo, T. *Macromol. Chem. Phys.* **2002**, *203*, 727.
(18) Zanuy, D. Alemán, C. *Biomacromolecules* **2001**, *2*, 65.
(19) de Pablo, J. J.; Laso, M.; Suter, U. W. *J. Chem. Phys.* **1992**, *96*, 2395.

(20) Siepmann, J. I.; Frenkel, D. *Mol. Phys.* **1992**, *75*, 59.
(21) León, S.; Alemán, C.; Escalé, F.; Laso, M. *J. Comput. Chem.* **2001**, *22*, 162.
(22) Weiner, S. J.; Killman, P. A.; Case, D. A.; Singh, U. C.; Ghio, C.; Alagona, G.; Profeta, S.; Weiner, P. *J. Am. Chem. Soc.* **1984**, *106*, 765.
(23) (a) Orozco, M.; Luque, F. J. *J. Comput.-Aided Mol. Des.* **1990**, *4*, 411. (b) Orozco, M.; Alemán, C.; Luque, F. J. *Acta Chim. Hung.* **1993**, *130*, 695. (c) Armelin, E.; Alemán, C.; Puiggalí, J. *J. Org. Chem.* **2001**, *66*, 8076.
(24) (a) Ahumada, O.; Laso, M. *Macromolecules* **2002**, *35*, 262. (b) Padding, J. T.; Briels, W. J. *J. Chem. Phys.* **2001**, *114*, 8685. (c) Harmandaris, V. A.; Mavrantzas, V. G.; Theodorou, D. N. *Macromolecules* **2000**, *33*, 8062. (d) Harmandaris, V. A.; Mavrantzas, V. G.; Theodorou, D. N. *Macromolecules* **1998**, *31*, 7934.
(25) Pearlman, D. A.; Case, D. A.; Caldwell, J. W.; Ross, W. S.; Cheatham, T. W., III; Ferguson, D. M.; Seibel, G. L.; Singh, U. C.; Weiner, P. K.; Kollman, P. A. *Amber 4.1*; University of California: 1995.
(26) (a) Karaborni, S.; Toxvaerd, S. *J. Chem. Phys.* **1992**, *96*, 5505. (b) Padilla, P.; Toxvaerd, S. *J. Chem. Phys.* **1991**, *95*, 509. (c) Schuler, L. D.; Daura, X.; van Gunsteren, W. F. *J. Comput. Chem.* **2001**, *22*, 1205. (d) RosiSchwartz, B.; Mitchell, G. R. *Polymer* **1996**, *37*, 1857.
(27) *Cerius*^{2} *1.6*; Molecular Simulations Inc.: Burlington, MA.
(28) Widmann, A. H.; Laso, M.; Suter, U. W. *J. Chem. Phys.* **1995**, *102*, 5761.
(29) Leontidis, E.; de Pablo, J. J.; Suter, U. W. *Adv. Polym. Sci.* **1994**, *116*, 283.

BM025702Q